Molecular Channels

DOI: 10.1002/anie.201002564

# Design of a Gated Molecular Proton Channel**

*Wei Gu, Bo Zhou, Tihamér Geyer, Michael Hutter, Haiping Fang,* and Volkhard Helms**

The generation of an electrochemical pH gradient across biological membranes using energy from photosynthesis and respiration provides the universal driving force in cells for the production of adenosine triphosphate (ATP), the energy unit of life.[1] Creating such an electrochemical potential requires the transportation of protons against a thermodynamic gradient. In biological proton pumps, chemical energy is used to induce protein conformational changes during each catalytic cycle where one or a few protons are pumped against a proton concentration gradient across the membrane. On the other hand, membrane channels also exist that mediate continuous particle exchange and may be switched between open and closed states.[2–7] Being able to design nanochannels with similar functions would be of great importance for creating novel molecular devices with a wide range of applications such as molecular motors,[8–11] fuel cells,[12] rechargeable nanobatteries that provide energy to other nanomachines,[13] and the generation of locally and temporally controlled pH jumps on microfluidic chips.

Despite its importance, the design of controllable mass transportation is still a great challenge.[14–17] Osmosis-driven transport found in many systems provides the easiest solution to the passive transport of substrates.[2] However, establishing an electrochemical potential requires gating segments to prevent backflow because a nongated channel cannot maintain a chemical potential. In many bionanomachines that conduct efficient and selective mass transportation, such as cytochrome c oxidase and $Na^+/H^+$ antiporter, the gating properties are controlled by conformational changes of the channel upon substrate binding and release[2–7] (for a detailed explanation see the Supporting Information).

Inspired by these observations, we present here the design of a gated molecular proton channel that can efficiently transport protons under electric fields with or against a concentration gradient. More importantly, the transportation is switchable and backflow can be prevented kinetically even when the external energy source is switched off. Inspired by analogous biological systems,[2,3] this design uses a rotatable chemical group attached to the inner wall of a nanopore as a gate and the external electric field as the energy source. The binding and release of a proton leads to the opening/closing of the gate (rotation of the functional group) under the external electric field and therefore controls the conduction of protons. In contrast to ligand-gated channels in biology, the ligand that induces the opening of the channel and the transported substrate are identical.

As model systems, we used uncapped armchair single-walled carbon nanotubes. Although proton transfer through nanochannels like carbon nanotubes can be very efficient,[18] a bare nanochannel without a switchable gate transfers protons in either direction making it hard to control the flow. To create a molecular switch that can be controlled externally, an acetic acid molecule is chemically attached to the inner wall of the nanochannel. Recent experimental advances make the decoration of the inner wall of carbon nanotubes possible.[19] Acetic acid is an analogue of aspartic acid, which acts as a molecular switch in many biological channels.[2,3,6,20] Recent work has revealed the protonation properties of aspartic acid and its role in transporting biological substrates.[2,21,22] Often, the protonation state of aspartic acid changes as a result of substrate binding. This leads to a conformational change of the channel that opens the channel to transport the corresponding substrates. After the substrates are released, the protonation state of the aspartic acid and the conformation of the channel recover to that of the unbound state to be ready for the next transport cycle and, very importantly, to close the channel to prevent reverse transport.

In our design, a graphite sheet is placed at one end of the nanochannel to separate the simulation system into two parts and prevent any exchanges between the upper and lower parts, except those through the nanochannel. Furthermore, an electric field is applied along the tube axis at different strengths (direction: top to bottom). Initially, a hydronium ion is randomly placed in the upper part of the system. Because of periodic boundary conditions, molecules leaving the box at one side will enter simultaneously on the opposite side. Details of the system setup are shown in Figure 1 a,b.

We performed a first series of molecular dynamics (MD) simulations for nanotubes with two different diameters with an acetic acid moiety as the rotating group and under different electric fields. Unlike ion transport, which can be

[*] Dr. W. Gu, Dr. T. Geyer, Dr. M. Hutter, Prof. Dr. V. Helms
Zentrum für Bioinformatik, Universität des Saarlandes
66041 Saarbrücken (Germany)
Fax: (+49) 681-302-64180
E-mail: volkhard.helms@bioinformatik.uni-saarland.de
B. Zhou, Prof. Dr. H. Fang
Shanghai Institute of Applied Physics, Chinese Academy of Sciences
PO Box 800-204, Shanghai 201800 (China)
E-mail: fanghaiping@sinap.ac.cn
Dr. W. Gu
Center of Computational Biology, College of Life Sciences
Nankai University, Tianjin 300071 (China)
B. Zhou
Graduate School of the Chinese Academy of Sciences
Beijing 100080 (China)

[**] This work was supported by the DFG (grant He3875/9-1), the PNNL (project EMSL GC 20896), the BMBF (grant CHN08/028), the NNSFC (grant 10825520), and the NBRPC (grant 2007CB936000). NWchem Version 4.7, as developed and distributed by the Pacific Northwest National Laboratory (PNNL), Richland, WA (USA), and funded by the U.S. Department of Energy, was used for some of the calculations.

Supporting information for this article is available on the WWW under http://dx.doi.org/10.1002/anie.201002564.

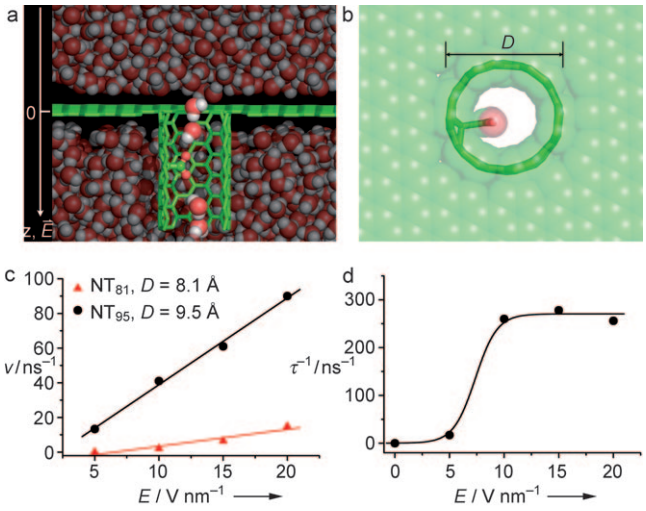


***Figure 1.*** a) Side view of the simulated system. The graphite sheet and carbon nanotube are represented using stick models. Acetic acid is shown in "ball-and-stick" form (green: carbon atoms and bonds, red: oxygen atoms). Water molecules are shown as space-filling models with the oxygen atoms as red spheres and the hydrogen atoms as white spheres. The white arrow denotes the $z$ axis and the direction of the electric field. 0 indicates the position of $z = 0$. b) Top view of the system (water not shown). c) Proton conducting rate $\nu$ in different simulations for two pore diameters $D$ at four different electric fields $E$. d) Intrinsic proton conducting rate in simulations of $NT_{95}$ under different electric fields. In (c) and (d), circles and triangles represent the data points, and solid curves show the fitted linear (in c) and sigmoid (in d) functions.

studied by classical MD simulation,[23,24] we used here the Q-HOP[25] method to address proton transfer in the simulations. Figure 1c shows the proton conducting rates (defined as the number of protons transported through the nanochannel per nanosecond). The rates range from a few protons per nanosecond to nearly 100 protons per nanosecond for different setups, showing that protons are conducted very rapidly under reasonable electric fields. There is a clear trend that the wider nanochannel ($D = 9.5$ Å, later referred to as $NT_{95}$) conducts protons faster. The conducting rate of $NT_{95}$ is about one order of magnitude greater than that of the narrower nanochannel ($D = 8.1$ Å, later referred to as $NT_{81}$). Stronger electric fields also result in higher conducting rates. When the electric field was increased from 5 $V\,nm^{-1}$ to 20 $V\,nm^{-1}$, the conducting rate increased nearly linearly in both $NT_{95}$ and $NT_{81}$ systems.

We note that the absolute values of the conducting rates partly depend on the time the proton takes to diffuse to the entrance and enter the tube. This time varies according to the system dimensions. We characterized the "pure" conducting capabilities of the designed channels as follows. An intrinsic conducting rate was defined as the reciprocal of the average "passing time" $\tau$ (passing time: time from when a proton enters the channel at the top until it leaves the channel at the bottom). $\tau$ was derived by fitting the number of transfer events with different passing times to an exponential function (see the Supporting Information). Figure 1d shows the intrinsic conducting rate of $NT_{95}$ under different electric fields. If one also considers that the rate should be zero when no field is applied, the data points can be nicely fitted to a sigmoid function. The rate increases slowly when the electric field is less than 5 $V\,nm^{-1}$, then boosts rapidly between 5 $V\,nm^{-1}$ and 10 $V\,nm^{-1}$, and saturates at fields stronger than 10 $V\,nm^{-1}$. This shows a clear "switching" behavior of the channel under different electric fields. For $NT_{81}$, the intrinsic conducting rate could only be reliably fitted for the simulation with the strongest electric field of 20 $V\,nm^{-1}$. The rate (86.2 $ns^{-1}$) is about one-third of that in $NT_{95}$ under the same field. In the other simulations for $NT_{81}$ with weaker fields, the numbers of transfer events were too small for this type of analysis.

To provide an atomistic understanding of the designed nanochannels, Figure 2 shows a detailed mechanism of proton conduction based on snapshots of one complete conduction process. In Step 0, the proton diffuses to the top of the channel via several water molecules and enters the nanochannel (not shown in Figure 2). In Step 1, the proton is transferred to the acetic acid. In Step 2, the protonation, which introduces an asymmetric charge distribution, triggers

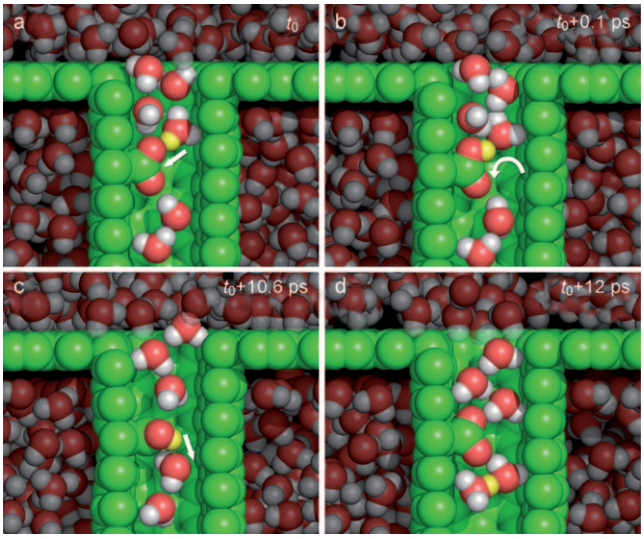


***Figure 2.*** Mechanism of gated proton conduction in the designed proton channels from snapshots of a complete conduction process (space-filling model; oxygen atoms: red, carbon atoms: green, hydrogen atoms: white). The proton that is being transferred in each step is colored yellow. a) Step 1: the proton is being transferred to the acetic acid. b) Step 2: the protonated acetic acid is rotating around the C–C bond under the electric field. c) Step 3: the proton is being transferred to a water molecule on the other side of the acetic acid. d) Step 4: after releasing the proton, the acetic acid returns to the resting position (as in Step 1).

acetic acid to rotate around the C–C bond under a sufficiently strong electric field by about 90 to 180°. In Step 3, the proton reaches a favorable transfer geometry to another water molecule on the other side of the acetic acid and is then transferred to that water molecule. In Step 4, after releasing the proton, the deprotonated acetic acid with symmetric charge distribution returns to its resting position either by rotating backwards or forwards depending on the rotation angles in Step 2, regardless of the electric field.

  

We also calculated the average "entering time" $\tau'$ (see the Supporting Information). The entering time is defined as the time interval between the point when a proton leaves the nanochannel at the bottom and the time when it enters the nanochannel from the top again. $\tau'$ reflects the average time of Step 0 and $\tau$ reflects the average time of Steps 1–3. For wider channels under stronger electric fields, that is, $NT_{95}$ with fields of 10, 15, and 20 $V\,nm^{-1}$, $\tau'$ (7.5, 5.8, and 4.0 ps, respectively) was larger than $\tau$ (3.8, 3.6, and 3.9 ps, respectively). In contrast, when the channels were narrower channels or the applied field weaker, that is, $NT_{81}$ with a field of 20 $V\,nm^{-1}$ and $NT_{95}$ with a field of 5 $V\,nm^{-1}$, $\tau'$ (2.7 and 4.8 ps, respectively) was shorter than $\tau$ (11.6 and 58.4 ps, respectively). These results indicate that, as expected, Step 0 is the rate-limiting step for wider channels under stronger electric fields, whereas in the other cases, Steps 1–3 are rate-limiting (especially Steps 2 and 3). In Step 2, the acetic acid group has to overcome the steric interaction with the inner wall. In Step 3, the release of the proton also requires surmounting the larger $pK_a$ of acetic acid. Density distributions of the protons along the tube axis show that Steps 2 and 3 are more difficult (i.e. take longer) for weaker fields or/and narrower tubes (see the Supporting Information).

In a thermodynamic sense, the pH gradient generated by an electrochemical potential across a separation layer is determined by the Nernst equation. In the present case, the electrical potential also affects the mobility of the rotating group, the gate. The strength of the electric field that is required to open the gate (i.e. to overcome the barriers of Steps 2 and 3) also reflects the capability of the gated channel to kinetically block unwanted backflow. In other words, it reflects the maximum pH gradient a certain channel can maintain. We have tested channels with different gate setups: 1) with a longer rotatable group and/or with a wider channel to reduce the rotation barrier; 2) with a rotatable group that has a smaller $pK_a$ (details given in the Supporting Information). In all cases, proton passage is possible at lower electric fields than before. Thus, as shown in Figure 3, changing the gate setup makes it possible to tune the required electric field for proton conductance. This, therefore, allows the tailored generation of specific pH gradients through the selection of a gate setup that can kinetically maintain a certain maximum pH gradient.

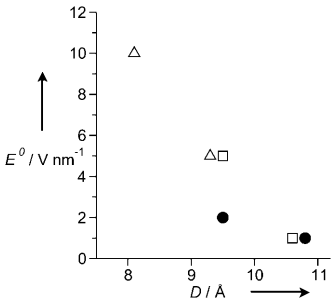


***Figure 3.*** Strength of the electric field $E^0$ required to observe proton passage within a simulation time of 1 ns for different gate setups; $D$ = diameter of the channel. △ = $COO^-$, □ = $CH_2COO^-$, ● = $CF_2COO^-$.

In summary, we have shown that the designed nanochannels can conduct protons in a very efficient way when a suitable electric field is applied. Analyzing the intrinsic conducting rate proves that these devices are also switchable. The opening of the gate requires both a strong electric field and the binding of a proton. When the electric field is small or turned off, the conduction of protons is turned off as a result of the steric clash between the acetic acid and the tube inner wall and because of its higher $pK_a$. Since the designed channel is "switched on" under stronger fields and "switched off" under weaker (or no) fields, it is possible to control the direction of the conduction, and therefore establish and kinetically maintain a chemical potential across the two sides of the devices. The magnitude of the potential is controllable by adjusting the chemical properties of the rotating group and the diameter of the channel.

## Computational Methods

The designed channels were solvated in boxes of SPC/E water molecules[26] with dimension 4.5 nm, 4.5 nm, and 3.8 nm along the $x$, $y$, and $z$ axes. The tube axis was parallel to the $z$ axis. Q-HOP MD simulations[25] were performed for each system at different longitudinal electric field in the direction $z_-$ to $z_+$. In total 25 simulations were performed up to a length of 1.0 to 1.5 ns; the total length was 26.8 ns. All simulations were performed in the NVT ensemble using a modified version of the NWChem 4.7 package[21,27] employing the AMBER99 force field.[28] All water molecules as well as the acetic acid residues were considered as possible donor/acceptors. All protons of the water molecules were transferable. We constrained the positions of the graphite layer and carbon atoms at the inlet and the outlet of the tube. Scanning for possible proton-transfer events was performed every 10 steps and snapshots were also recorded every 10 steps to track all hopping events.

Received: April 29, 2010
Revised: October 7, 2010
Published online: December 17, 2010

**Keywords:** active transport · carbon nanotubes · molecular dynamics · proton channels · proton transfer

[1] P. Mitchell, *Nature* **1961**, *191*, 144.
[2] I. T. Arkin, H. F. Xu, M. O. Jensen, E. Arbely, E. R. Bennett, K. J. Bowers, E. Chow, R. O. Dror, M. P. Eastwood, R. Flitman-Tene, B. A. Gregersen, J. L. Klepeis, I. Kolossvary, Y. B. Shan, D. E. Shaw, *Science* **2007**, *317*, 799.
[3] H. Michel, *Proc. Natl. Acad. Sci. USA* **1998**, *95*, 12819.
[4] H. Luecke, B. Schobert, H. T. Richter, J. P. Cartailler, J. K. Lanyi, *Science* **1999**, *286*, 255.
[5] S. Iwata, C. Ostermeier, B. Ludwig, H. Michel, *Nature* **1995**, *376*, 660.
[6] C. Hunte, E. Screpanti, M. Venturi, A. Rimon, E. Padan, H. Michel, *Nature* **2005**, *435*, 1197.
[7] C. Olesen, M. Picard, A.-M. L. Winther, C. Gyrup, J. P. Morth, C. Oxvig, J. V. Moller, P. Nissen, *Nature* **2007**, *450*, 1036.
[8] R. K. Soong, G. D. Bachand, H. P. Neves, A. G. Olkhovets, H. G. Craighead, C. D. Montemagno, *Science* **2000**, *290*, 1555.
[9] M. Schliwa, G. Woehlke, *Nature* **2003**, *422*, 759.
[10] M. G. L. van den Heuvel, C. Dekker, *Science* **2007**, *317*, 333.
[11] F. Xia, W. Guo, Y. Mao, X. Hou, J. Xue, H. Xia, L. Wang, Y. Song, H. Ji, Q. Ouyang, Y. Wang, L. Jiang, *J. Am. Chem. Soc.* **2008**, *130*, 8345.

  

[12] K. D. Kreuer, S. J. Paddison, E. Spohr, M. Schuster, *Chem. Rev.* **2004**, *104*, 4637.
[13] R. Ballardini, V. Balzani, A. Credi, M. T. Gandolfi, M. Venturi, *Acc. Chem. Res.* **2001**, *34*, 445.
[14] I. M. Bennett, H. M. V. Farfano, F. Bogani, A. Primak, P. A. Liddell, L. Otero, L. Sereno, J. J. Silber, A. L. Moore, T. A. Moore, D. Gust, *Nature* **2002**, *420*, 398.
[15] S. Joseph, R. J. Mashl, E. Jakobsson, N. R. Aluru, *Nano Lett.* **2003**, *3*, 1399.
[16] M. Majumder, X. Zhan, R. Andrews, B. J. Hinds, *Langmuir* **2007**, *23*, 8624.
[17] C. A. Wraight, *Biochim. Biophys. Acta Bioenerg.* **2006**, *1757*, 886.
[18] C. Dellago, M. M. Naor, G. Hummer, *Phys. Rev. Lett.* **2003**, *90*, 105902.
[19] T. Kyotani, S. Nakazaki, W.-H. Xu, A. Tomita, *Carbon* **2001**, *39*, 782.
[20] J. C. Xu, G. A. Voth, *Proc. Natl. Acad. Sci. USA* **2005**, *102*, 6795.
[21] W. Gu, T. Frigato, T. P. Straatsma, V. Helms, *Angew. Chem.* **2007**, *119*, 2997; *Angew. Chem. Int. Ed.* **2007**, *46*, 2939.
[22] W. Gu, V. Helms, *J. Am. Chem. Soc.* **2009**, *131*, 2080.
[23] W. Im, B. Roux, *J. Mol. Biol.* **2002**, *322*, 851.
[24] A. Aksimentiev, K. Schulten, *Biophys. J.* **2005**, *88*, 3745.
[25] M. A. Lill, V. Helms, *J. Chem. Phys.* **2001**, *115*, 7993.
[26] H. J. C. Berendsen, J. R. Grigera, T. P. Straatsma, *J. Phys. Chem.* **1987**, *91*, 6269.
[27] T. P. Straatsma, M. Philippopoulos, J. A. McCammon, *Comput. Phys. Commun.* **2000**, *128*, 377.
[28] W. D. Cornell, P. Cieplak, C. I. Bayly, I. R. Gould, K. M. Merz, D. M. Ferguson, D. C. Spellmeyer, T. Fox, J. W. Caldwell, P. A. Kollman, *J. Am. Chem. Soc.* **1995**, *117*, 5179.

  